





Article

Path Planning for Autonomous Underwater Vehicles (AUVs) Considering the Influences and Constraints of Ocean Currents

Ziming Chen ¹, Jinjin Yan ^{1,2,*}, Ruen Huang ², Yisong Gao ², Xiuyan Peng ¹ and Weijie Yuan ³

¹ College of Intelligent Systems Science and Engineering, Harbin Engineering University, Harbin 150001, China; ziming.chen@hrbeu.edu.cn (Z.C.); pengxiuyan@hrbeu.edu.cn (X.P.)

² Qingdao Innovation and Development Center, Harbin Engineering University, Qingdao 266400, China; ruen.huang@hrbeu.edu.cn (R.H.); gys2001@hrbeu.edu.cn (Y.G.)

³ Department of Electrical and Electronic Engineering, Southern University of Science and Technology, Shenzhen 518055, China; yuanwj@sustech.edu.cn

* Correspondence: jinjin.yan@hrbeu.edu.cn; Tel.: +86-153-2115-5969

Abstract: Ocean currents pose a significant challenge in the path planning of autonomous underwater vehicles (AUVs), with conventional path-planning algorithms often failing to effectively counter these influences. In response to this challenge, we propose a path-planning algorithm that can consider the influences and constraints of ocean currents, which leverages the strengths of two widely employed path-planning algorithms, A* and the genetic algorithm (GA), to account for the influences of ocean currents on the planned paths. Specifically, it enhances the initial population generation, formulates a fitness function tailored to ocean current conditions, and employs an adaptive mutation approach to enhance population diversity and stability. By utilizing simulated and real-world ocean current datasets, we validated the feasibility of the proposed algorithm with quantitative metrics. The results demonstrate that in comparison to conventional methods, the new algorithm can deal with the influences and constraints of ocean currents in AUV path planning, resulting in notable enhancements in path smoothness, energy efficiency, and safety.

Keywords: AUV; pathplanning; ocean currents; genetic algorithm; path performance evaluation



Citation: Chen, Z.; Yan, J.; Huang, R.; Gao, Y.; Peng, X.; Yuan, W. Path Planning for an Autonomous Underwater Vehicle (AUV) Considering the Influences and Constraints of Ocean Currents. *Drones* **2024**, *8*, 348. <https://doi.org/10.3390/drones8080348>

Academic Editor: Pablo Rodríguez-Gonzálvez

Received: 4 July 2024
Revised: 23 July 2024
Accepted: 24 July 2024
Published: 26 July 2024



Copyright: © 2024 by the authors. Licensee MDPI, Basel, Switzerland. This article is an open access article distributed under the terms and conditions of the Creative Commons Attribution (CC BY) license (<https://creativecommons.org/licenses/by/4.0/>).

1. Introduction

The autonomous underwater vehicle (AUV) is a specialized type of unmanned underwater vehicle (UUV) that equips advanced guidance systems and on-board energy storage, thereby enabling sustained autonomous operations lasting from several hours to multiple days [1]. This autonomy enables AUVs to undertake tasks within intricate marine environments that are typically inaccessible or pose challenges for human intervention. A noteworthy illustration of AUV capabilities can be observed in the case of the Bluefin-21, owned by General Dynamics (a U.S. company), which effectively conducted an independent search for debris from the ill-fated Malaysia Airlines MH370 passenger jet in 2014 [2].

In the autonomous task of AUVs, path planning is paramount, as it is necessary to determine an optimal and obstacle-free path to reach the desired destination. In other words, path planning serves as a foundational technology for AUVs, exerting substantial influences on the efficacy and applicability of AUV deployments across diverse scenarios [3]. Compared to the path-planning tasks of unmanned aerial vehicles (UAVs) and unmanned ground vehicles (UGVs), AUVs operate within highly intricate underwater domains, which differ significantly from the conditions encountered by terrestrial and aerial vehicles. The presence of ocean currents exerts non-negligible influences on the path-planning process for AUVs. It is noteworthy that in previous research endeavors focused on AUV path planning, a relatively limited proportion of studies considered the factor of ocean currents [4]. Therefore, it is crucial that planned paths are optimized for

navigation in ocean current environments, which include creating smooth paths with minimized turning angles, avoiding dangerous high-speed ocean current areas to improve safety, and adhering to ocean current directions to maximize energy efficiency. Hence, the imperative arises to cultivate path-planning algorithms expressly tailored to AUVs, taking into account the influences and constraints of ocean currents.

A range of classical path-planning algorithms has been investigated for the autonomous navigation of AUVs, including Dijkstra [5], rapidly exploring random tree (RRT) [6], and artificial potential field (APF) [7]. Among these, A* is notably the most widely applied, persisting as a popular choice for AUV path planning [8]. Recent research continues to focus on A* to optimize AUV path planning, reflecting ongoing efforts to refine its application [8–12]. Intelligence-based algorithms such as ant colony optimization (ACO) [13] and particle swarm optimization (PSO) [14] have also gained traction in recent years. Additionally, evolutionary algorithms, with the genetic algorithm (GA) as a prominent representative, have emerged as a prevalent choice for path planning. The GA, in particular, is widely acknowledged for its effectiveness as an optimization technique in the domain of path planning [15]. Notably, various studies have undertaken the task of enhancing the GA to yield superior results. For instance, an enhanced GA variant has been developed to generate smoother and more cost-effective paths for UUVs [16]. To expedite convergence and refine path optimization, the GA incorporates the use of the chamfer operator [17]. Furthermore, in addressing the issue of premature convergence in AUV path planning, a combined approach involving adaptive crossover probability and mutation probability has been integrated into the GA [18].

The algorithms mentioned above can perform path planning of AUVs. Nevertheless, they exhibit notable limitations when referring to environmental conditions. For example, A* determines optimal solutions based on a heuristic search, but it is only suitable for simple environments. The GA can better adapt to complex search spaces, but it is more computationally resource-intensive and prone to fall into local optima. Ocean currents present a notable challenge in path planning of AUVs. Thus, algorithms for path planning of AUVs should not only be suitable for environments with ocean currents and reduce computational resource consumption but also have efficient search strategies for achieving global optimal solutions. In view of this, we argue that the integration of diverse path-planning algorithms could be a promising strategy, for instance, combining the GA with A*. The combination of different path-planning algorithms, as discussed in the outlook and future directions sections of reference [3], holds the potential to effectively address the path-planning challenges of AUVs.

In recent years, an increasing number of studies started to consider the influences of currents on AUV path planning [19–22]. These studies introduced simple ocean current models and integrated current dynamics into AUV path planning, enhancing the adaptability of AUV paths to the prevailing current conditions. However, these studies do not adequately simulate changes in currents around obstacles, resulting in inaccurate current representations in such areas. Moreover, the evaluation of these models has primarily occurred within simulated environments. In contrast, some studies use real-world ocean current observations to enable AUVs to navigate based on actual ocean currents [23]. Nonetheless, despite these advancements, the models still fail to address obstacle-related factors and do not meet the obstacle-avoidance requirements of AUVs. One approach incorporates an adaptive GA to obtain globally optimal paths and proposes a local path-planning method based on vector APF [24]. While this method has been tested with authentic ocean current data, it falls short in addressing issues such as path smoothness and adherence to AUV dynamics constraints. Another study integrates the GA with ACO and the simulated annealing (SA) algorithm to improve AUV path convergence and mitigate the risk of falling into local optima [25]. This research introduces an ocean current model to validate the adaptability of the algorithm to ocean currents, but it does not incorporate obstacles within the ocean current environment and does not address the effectiveness of obstacle avoidance within such conditions.

In summary, ocean currents significantly influence and constrain AUV path planning. Current research often does not fully address these complexities, as reliance on a single traditional algorithm typically falls short in dynamic underwater environments. To overcome these limitations, this paper proposes a novel path-planning algorithm for environments influenced by ocean currents. Inspired by the strengths of the A* algorithm in determining optimal solutions and the global optimization capabilities of the GA in complex settings, our approach integrates these into a fusion algorithm. The proposed algorithm combines the best features of both A* and GA, enhancing computational efficiency and reducing the risk of stagnation in local optima. It leverages the optimization capabilities of the GA to adapt to the dynamic and intricate underwater current environment. This innovative approach promises a more effective solution for AUV path planning in challenging oceanic conditions.

The main contributions are as follows:

1. A fusion algorithm that can consider the influences and constraints of ocean currents is proposed.
2. A more realistic ocean current model is designed and used to verify the effectiveness of the algorithm.
3. Based on requirements of AUV path planning in environments with ocean currents, cost and fitness functions are established.
4. We present new criteria for path comparison, quantitatively expressing the adaptability of a path to ocean currents, which can be used for more precise performance analysis of navigation paths of AUVs.

The rest of this article is organized as follows: Section 2 defines the problem of path planning in ocean current environments. Section 3 provides details of the proposed algorithm. Section 4 carries out experiments to verify the feasibility of the algorithm and offers a quantitative analysis and comparison of path performance. Finally, Section 5 concludes the research and discusses potential future work.

2. Problem Description

In this paper, we simplify the navigation environment by modeling it as a two-dimensional plane to simulate the fixed-depth navigation of an AUV. A navigation path (S) of an AUV can be represented as a series of waypoints, as shown in Equation (1):

$$S = \langle P_1, P_2, P_3, P_4 \cdots P_i \rangle \quad (1)$$

where P_i is the i th waypoint on the path, and each waypoint can be mapped onto a grid map.

The grid map consists of a series of cells, each representing a specific area, which can be assigned a value based on the characteristics of the area (e.g., the presence or absence of obstacles) [26]. The grid map is defined as a two-dimensional array M , where $M[i][j]$ represents the grid cell at the i -th row and j -th column, with each cell portraying a specific geographic or environmental characteristic. The value of a cell can be marked by two numbers: "0" or "1". If a grid unit is marked by "0", it indicates that this unit is passable, while "1" denotes a unit that is impassable (such as occupied by an obstacle).

2.1. Modeling of Ocean Currents

It is inappropriate to model ocean currents in a single, straightforward vector [27]. In this paper, we introduce a comprehensive ocean current model that encompasses two distinct types of currents: random currents and Lamb–Oseen vortices [28]. The former is generated using a normal distribution (Equations (2) and (3)). This approach introduces a level of complexity to the modeled currents that surpasses the simplicity of constant-speed currents.

$$C_{\theta_{i,j}} \sim N(\mu, \sigma^2) \quad (2)$$

where $C_{\theta_{i,j}}$ is the angle of the current at the position (coordinates are (i, j)) on the grid map. μ and σ are the mean and variance of the ocean current directions, respectively.

$$C_{V_{i,j}} \sim U(V_{min}, V_{max}) \quad (3)$$

where $C_{V_{i,j}}$ is the velocity of the ocean current at (i, j) . The velocity of the ocean current in the direction of x and y is (Equation (4)) as follows:

$$\begin{cases} vel_x = C_{V_{i,j}} \cdot \cos(C_{\theta_{i,j}}) \\ vel_y = C_{V_{i,j}} \cdot \sin(C_{\theta_{i,j}}) \end{cases} \quad (4)$$

The latter, the Lamb–Oseen vortex, is a well-established mathematical model that finds widespread application in simulating realistic ocean currents [23]. This model is typically represented as a two-dimensional, incompressible, viscous fluid, as expressed in Equation (5).

$$\begin{cases} V_{\theta}(r, t) = \frac{\Gamma}{2\pi r} \left(1 - e^{-\frac{r^2}{r_c^2(t)}} \right) \\ r_c(t) = \sqrt{4\nu t + r_c(0)^2} \end{cases} \quad (5)$$

where r denotes the radius, V_{θ} is the velocity of the ocean current, and $r_c(t)$ is the core radius of the vortex which changes over time. ν is the liquid viscosity, Γ is the vortex circulation, and $r_c(0)$ signifies the core radius at the initial time.

Although the vortex field may undergo a series of changes as time progresses, we assume that the vortex field is relatively stable during the traversal of an AUV, because when an AUV traverses such a region, the time difference of its passage is much smaller than the time in which significant changes in the vortex occur. Therefore, we can disregard the time-domain changes of the vortex field. Then, the term $-\frac{r^2}{r_c^2(t)}$ can be further simplified to $-\frac{r^2}{R_c^2}$, where R_c signifies the radius of the vortex core. Then, the $V_{\theta}(r, t)$ in Equation (5) becomes Equation (6):

$$V_{\theta}(r) = \frac{\Gamma}{2\pi r} \left(1 - e^{-\frac{r^2}{R_c^2}} \right) \quad (6)$$

It is important to highlight that many prior studies have either overlooked the consideration of obstacles within ocean currents or simply superimposed ocean currents onto obstacles. Such practices disregard the fact that currents around obstacles undergo alterations, creating erroneous modeling that the currents can freely traverse these obstacles. In path planning, however, the presence of currents around obstacles, even if they are relatively weak, is a factor that cannot be dismissed. Therefore, the ocean current model should be capable of adapting to obstacles, allowing for a more accurate modeling of currents around the periphery of obstacles.

In this paper, the velocity of positions (units) occupied by obstacles is set to zero. If the velocity at a position is non-zero but an obstacle is present within one unit on the Y axis, the vel_y component is set to zero while the vel_x component is retained. A similar approach is applied to the vel_x settings on the X axis. This method is outlined in Algorithm 1.

Algorithm 1 Ocean currents modeling around obstacles.

```

1: if  $O(x, y) == 1$  then
2:    $vel\_x(x, y) \leftarrow 0$ 
3:    $vel\_y(x, y) \leftarrow 0$ 
4: end if
5: if  $O(x, y) == 0$  then
6:   if  $O(x, y + 1) == 1$  or  $O(x, y - 1) == 1$  then
7:      $vel\_y(x, y) \leftarrow 0$ 
8:   end if
9:   if  $O(x + 1, y) == 1$  or  $O(x - 1, y) == 1$  then
10:     $vel\_x(x, y) \leftarrow 0$ 
11:   end if
12: end if

```

2.2. Mechanical Modeling of AUV

As this paper primarily discusses path planning for AUVs at a fixed depth, we assume that the AUV operates within a two-dimensional plane. To simplify the model and focus on the core issue, this study does not consider complex dynamics such as sideslip or rolling that the AUV may encounter during operation. Hence, we regard the AUV as moving steadily and linearly within the horizontal plane, disregarding any dynamic changes in the vertical direction and any tilting or rotation in three-dimensional space. This assumption helps us to more accurately analyze and optimize the path-planning problem at the specified depth. In modeling the mechanical characteristics of the AUV (Figure 1), we take into account the effects of the propulsion force F_p and rotational torque M_p , as well as the resistance forces F_d and M_d . The distance (d_i) is defined as the Euclidean distance between the center of the AUV at its current moment and the center of the AUV at its subsequent moment. Similarly, the angle ($\Delta\varphi_i$) is the angular difference between the current orientation of the AUV at the current moment and its orientation at the subsequent moment.

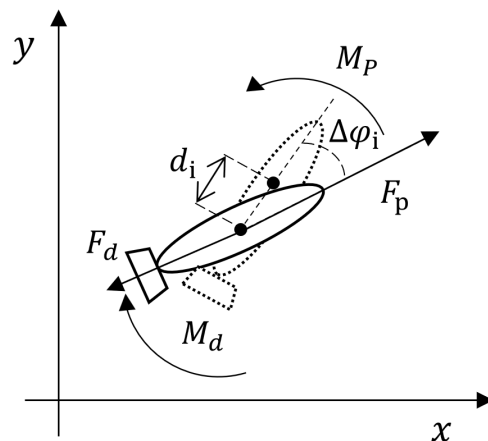


Figure 1. Illustration of AUV movements on a plane.

The energy consumption of the AUV encompasses both the energy expended due to the propulsion force and the energy consumed by the rotational torque. Therefore, the energy consumption along the path (S) can be expressed as depicted in Equation (7):

$$E = \sum_{i=1}^{n-1} \left((k_v \cdot v^2 + m \cdot a) \cdot d_i + (k_\omega \cdot (v \cdot \frac{\Delta\varphi_i}{d_i})^2 + (M_p - M_d)) \cdot \Delta\varphi_i \right) \quad (7)$$

where a is the linear acceleration, m is the mass of the AUV, v is velocity, ω is angular velocity, k_v is the linear velocity resistance coefficient, and k_ω is the drag coefficient of angular velocity.

If we assume that v and M_p are constants, an increase in $\Delta\phi_i$ corresponds to a rise in E . In simpler terms, a planned path with excessively large turning angles or frequent turns will consume more AUV energy for direction adjustments, posing greater control challenges. It is essential to note that AUVs cannot engage in high-frequency or large-scale steering maneuvers due to their operational constraints [29]. This means that paths with sharp turning angles, which correspond to small radii of curvature, are not achievable. Therefore, the planned path should prioritize smoothness, incorporating gradual changes in direction to adhere to these limitations.

2.3. Influences of Ocean Currents

The progress of AUV is usually affected by the force of the ocean current (Figure 2).

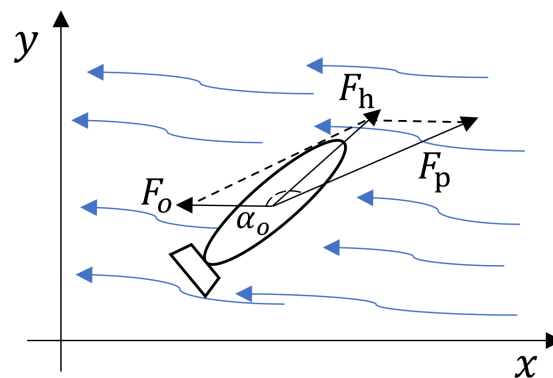


Figure 2. Illustration of AUV influenced by ocean currents.

In the above figure, F_o represents the force of the ocean current, F_p is the maximum propulsion force of the AUV, and F_h is the resultant force in the direction of travel. The angle between F_o and F_p , denoted as α_o , allows us to calculate the magnitude of F_h according to the parallelogram law (Equation (8)):

$$\|\vec{F}_h\| = \sqrt{\|\vec{F}_o\|^2 + \|\vec{F}_p\|^2 + 2\|\vec{F}_o\|\|\vec{F}_p\|\cos(\alpha_o)} \quad (8)$$

This equation demonstrates that when the speed of the ocean current is constant (F_o constant) and the maximum propulsion force F_p is fixed, the resultant force F_h increases as the propulsion direction more closely aligns with the current direction, indicated by a larger value of $\cos(\alpha_o)$. Therefore, the more aligned the propulsion direction is with the current, the stronger the propulsion power is for the same amount of thrust, resulting in energy savings. In other words, the closer the alignment between the path and the ocean current, the less additional energy is needed. If the planned path enables the AUV to move in the direction of the ocean current and diminishes the proportion of paths against the current, the AUV can conserve energy and achieve a longer sailing distance.

3. The Proposed Path-Planning Algorithm

Traditional algorithms often struggle to adapt to environments with ocean currents. In this paper, we present a path-planning algorithm designed to tackle the challenges posed by ocean currents. The algorithm framework, illustrated in Figure 3, consists of four fundamental components: inputs, an enhanced A*, an enhanced GA, and output.

This algorithm initiates by taking ocean maps and current data as inputs to facilitate path planning. The path planning employs an enhanced A* algorithm, which we refer to as the enhanced A*. This method is specifically modified to optimize several cost factors that the traditional A* does not adequately address. These include distance costs from obstacles, angle costs of ocean currents, and distance cost. The results obtained from the enhanced A* are a series of waypoints.

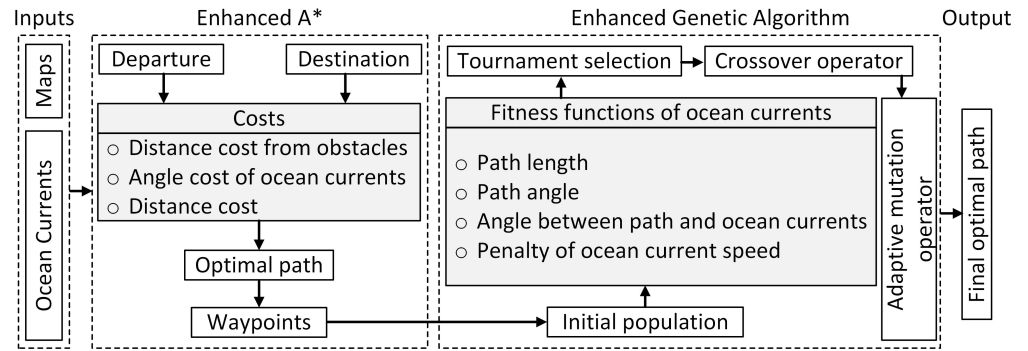


Figure 3. Framework of the proposed algorithm.

The use of the GA in path planning requires significant resources for comprehensive environmental exploration and ongoing generation of new paths. However, when planning paths for AUVs, it is crucial to account for the hardware and communication limitations. For the GA, choosing an effective initial population method can significantly reduce computational resource usage by generating a high-quality initial population [30]. To this end, the waypoints derived from the enhanced A* algorithm are used as the initial population in our GA approach, thus reducing the computational load typically associated with a GA that starts with randomly generated initial populations. This strategy helps avoid the extensive computational costs normally incurred with such random initial setups.

Furthermore, we tailor the fitness functions of the GA to address the challenges posed by ocean currents. These functions evaluate the paths based on their length, angle, angle deviation from ocean currents, and penalties associated with ocean current speed. Finally, the initial populations undergo further refinement through tournament selection, crossover operations, and adaptive mutation. To prevent premature algorithm convergence and steer clear of local optimal solutions, we introduce adaptive mutation operators and tournament methods. Ultimately, our approach yields the optimal path that effectively adapts to the presence of ocean currents.

3.1. Enhanced A* Algorithm

The traditional A* algorithm primarily considers path length as the cost metric, which is insufficient for navigating environments influenced by ocean currents. To address this limitation, we propose a more comprehensive cost function that includes both the distance cost from obstacles and the angle cost associated with ocean currents. This enhanced cost function not only improves path safety but also reduces fuel consumption.

The distance cost from obstacles is quantified as (Equation (9)):

$$\begin{cases} d(P_i, O_i) = \sqrt{((x_i - o_{x_i})^2 + (y_i - o_{y_i})^2)} \\ OP_i = \frac{\omega_{op}}{\min\{d(P_i, O_i)\} + \epsilon} \end{cases} \quad (9)$$

where $P_i(x_i, y_i)$ represent consecutive waypoints. $O_i(o_{x_i}, o_{y_i})$ is an obstacle point, and $d(P_i, O_i)$ signifies the distance between the current path and all obstacles. OP_i indicates the cost associated with the closest obstacle to the current point. ω_{op} serves as the obstacle penalty weight. ϵ is a small positive number added to prevent division by zero during the planning process.

The cost of the ocean current angle is (Equation (10)):

$$\begin{cases} T(a, b) = \arctan\left(\frac{a}{b}\right) \\ \theta(V_k) = T(v_{y_k}, v_{x_k}), \quad k \in \{i, j\} \\ \theta(P_i, P_j) = T(y_j - y_i, x_j - x_i) \\ AP_i = \alpha|\theta(P_i, P_j) - \theta(V_j)| + \beta|\theta(P_i, P_j) - \theta(V_i)| \end{cases} \quad (10)$$

where $\theta(P_i, P_j)$ is the direction of the velocity at the current waypoint and $\theta(V_i)$ and $\theta(V_j)$ are the directions of the current and next current velocities at the waypoint. α and β are the weighting coefficients, which represent the weights of the current direction of neighboring points and the current direction of the current point, respectively.

By incorporating the cost associated with the angle of the ocean current into the cost function $f(P_i)$, the resulting path aligns more closely with the direction of the ocean current, effectively maintaining a greater distance from obstacles. The comprehensive cost function for the enhanced A* algorithm is expressed as Equation (11):

$$f(P_i) = g(P_i) + h(P_i) + OP_i + AP_i \quad (11)$$

3.2. Encoding Method and Initial Population

We utilize a real number encoding method, treating the path of the enhanced A* divided into discrete waypoints and further employing them as individuals (Equation (12)).

$$Population = \{M_1(S_{A^*}), M_2(S_{A^*}), \dots, M_i(S_{A^*})\} \quad (12)$$

where A^* is the path of the enhanced A* algorithm, M is the set of waypoints that are divided from the A^* , and M_i is an individual that will be replicated to generate a population.

The initial population method presented herein significantly alleviates the computational load by focusing exclusively on path calculations within the population and their adjacent waypoints, circumventing the necessity to explore global points. Consequently, this method significantly reduces the computational burden associated with the GA, making it better suited to the constraints of limited computational resources in AUV path planning.

3.3. Fitness Function and Tournament Selection

To address the path-planning requirements of AUVs in ocean currents, we introduced a fitness function tailored to the unique characteristics of these currents. This function consists of four indicators, including path length (L), path smoothness (H), alignment of path direction with that of ocean currents (C), and avoidance of high-speed ocean currents (pcs). Together, these indicators filter the population to retain individuals that demonstrate greater adaptability to ocean conditions, thus ensuring optimal path selection.

Path length (L): considering a path composed of n waypoints, we calculate the distances between adjacent points to determine the path length, as shown in Equation (13):

$$L = \sum_{i=1}^{n-1} \sqrt{(x_{i+1} - x_i)^2 + (y_{i+1} - y_i)^2} \quad (13)$$

where L is the length of the path.

Path smoothness (H): This indicator is ascertained through the summation of the angles formed between each successive path segment (Equation (14)). In particular, it is built upon a concept named the turn angle. As shown in Figure 4, there are three waypoints on the path, $P_{i-1}(x_{i-1}, y_{i-1})$, $P_i(x_i, y_i)$, and $P_{i+1}(x_{i+1}, y_{i+1})$, and the path length between P_{i-1} and P_i is $L1$, and that between P_i and P_{i+1} is $L2$. Then, the turn angle (θ_i) of this path is the angle between $\overrightarrow{P_{i-1}P_i}$ and $\overrightarrow{P_iP_{i+1}}$ (Equation (14)). It is essential to underscore that the value of H is negatively correlated with path smoothness, that is, smoother paths have a lower value.

$$H = \sum_{i=1}^{n-2} \arccos\left(\frac{\overrightarrow{P_{i-1}P_i} \cdot \overrightarrow{P_iP_{i+1}}}{\|\overrightarrow{P_{i-1}P_i}\| \|\overrightarrow{P_iP_{i+1}}\|}\right) \quad (14)$$

Alignment of path direction with ocean current (C): At each waypoint, an angle can be calculated based on the angles between the current waypoint and the directions of the ocean current. This indicator is the summation of all these angles (Equation (15)). The definitions of $\theta(V_i)$ and $\theta(P_i, P_j)$ are explained in Equation (10). Essentially, it signifies that

if an AUV path aligns with the direction of the ocean current, fuel consumption can be minimized. Consequently, this indicator also serves as a measure of energy efficiency.

$$C = \sum_{i=1}^{n-1} \cos(\theta(V_i) - \theta(P_i, P_j)) \quad (15)$$

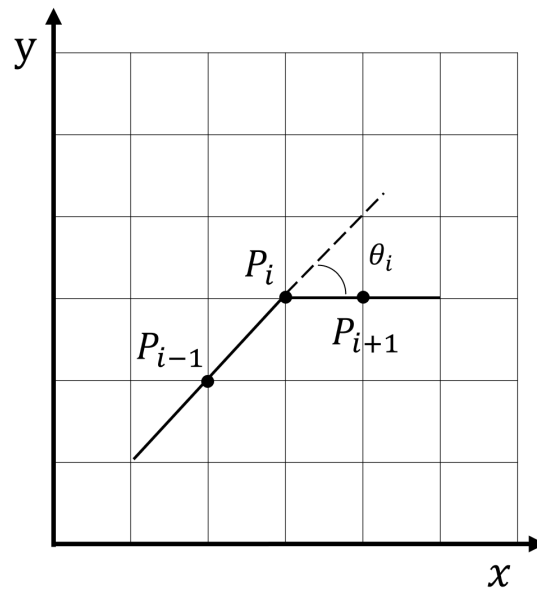


Figure 4. Illustration of path angle.

Avoidance of high-speed ocean currents (*pcs*): To enhance AUV safety and controllability in high-speed ocean currents, we incorporate a current speed penalty into the fitness function to indicate the avoidance of high-speed ocean currents. Firstly, we define a threshold (R). For each waypoint (P_i) on the path, we assess the current speed at this location and its subsequent one to determine if it exceeds R . If the speed surpasses R , we then add a penalty (denoted as *pcs*) to the ocean current speed. After examining all points in the path in this way, we compute a total penalty score. A lower penalty score indicates that the path is safer.

Considering the above scoring criteria, the total fitness score is (Equation (16)):

$$score = L \times W_1 + H \times W_2 - C \times W_3 + pcs \times W_4 \quad (16)$$

where W_1 , W_2 , W_3 , and W_4 are the weight coefficients, which can be adjusted based on the specific conditions of the ocean current.

3.4. Tournament Selection

We implement a tournament selection method to filter out individuals with high fitness while excluding those with lower fitness levels, thereby ensuring that the retained individuals exhibit exceptional fitness. The tournament selection process hinges on two key parameters: the desired number of individual and the tournament size.

Once these two parameters are determined, the algorithm proceeds by selecting high-performing individuals from the population and orchestrating a tournament selection round within this subgroup. This entails the random selection of the desired number of individuals from the subgroup, with each individual paired alongside their respective fitness score to create the tournament competitors. In this paper, we define fitness inversely: the higher the fitness, the lower the score. Therefore, the victor of the tournament is the individual with the lowest fitness score. This champion individual is then retained for subsequent stages of the algorithm.

This process is repeated iteratively until the number of victorious individuals reaches the specified target for entities. This iterative selection methodology fosters a competitive environment, ultimately resulting in the selection of the most adaptable individuals based on their performances.

3.5. Crossover Operator and Adaptive Mutation Operator

Before the crossover process, mutation operations are applied to each path individual M_i within the population. This strategy diversifies the paths of individuals, enriches the initial population, and promotes overall population diversity. Concurrently, a single-point crossover method is used, which involves randomly selecting a point (excluding the start and end points) along the parental path for crossover, resulting in the generation of offspring. This approach ensures that superior individuals, as previously mentioned, are bred to achieve the desired population count.

As for the mutation probability and process, a mutation probability m is defined, and each point P_i within an individual (excluding the start and end points) determines whether a mutation occurs based on this probability. If a mutation is triggered, it involves a random (one-unit) movement in both the X and Y directions. In particular, an integer dx is randomly selected from the set $\{-1, 0, 1\}$, and so is dy . Then, a new waypoint $P'_i(x_i + dx, y_i + dy)$ is computed. This process repeats until the newly generated waypoints no longer intersect with any obstacles.

Moreover, to enhance search efficiency and minimize disturbances, we implement an adaptive function to dynamically adjust the mutation rate. Numerous studies have demonstrated that an appropriate dynamic mutation rate can significantly enhance the performance of GA [31–33]. Initially, a higher mutation rate is employed to diversify the population and expand the exploration of the solution space, which helps avoid entrapment in local optima and accelerates the search process. As the algorithm progresses and the population begins to converge towards optimal solutions, a reduced mutation rate is applied to refine the search and reduce disruptions. The adaptive mutation function is defined according to the progress of the current generation (Equation (17)). With the increase generation, the mutation rate will decrease from the initial to the minimum mutation rate.

$$\text{mutation_rate} = \text{ini_rate} \times \left(1 - \frac{\text{cur_gen}}{\text{tot_gen}}\right) + \text{min_rate} \times \frac{\text{cur_gen}}{\text{tot_gen}} \quad (17)$$

where cur_gen denotes the current iterations, tot_gen denotes the total iterations, ini_rate is the initial mutation rate, and min_rate is the minimum mutation rate.

4. Experiment and Case Study

4.1. Experimental Scenarios

To test and validate the performance and adaptability of our proposed algorithm, we conducted experiments using two distinct datasets: one comprises synthetic data and the other comprises authentic datasets. Due to the substantial cost associated with AUVs and in-ocean experiments, we opted for simulation-based experimentation.

The synthetic dataset consists of four scenarios (Figure 5), each spanning approximately 10,000 square meters. Although the obstacles in all four scenarios remain constant, there are variations in ocean currents. Specifically, random currents are employed in Figure 5a,c, while those in Figure 5b,d are three Lamb–Oseen vortices. We use the stream-lined diagrams to visually represent the ocean currents, in which arrow directions denote the currents direction and colors of streamline indicate the speed (blue representing low-speed regions and red indicating high-speed). Notably, ocean currents tend to circumvent rather than penetrate obstacles. This modeling approach is distinctly different from methods that either ignore the impact of obstacles on ocean currents or assume currents can intersect directly with obstacles. As a result, our simulations of ocean currents more ac-

curately reflect real-world scenarios. In the experiments with the synthetic datasets, the speed of the ocean current ranges from 0 to 5 m/s, and the mean and standard deviation of the ocean current direction are set at $\pi/4$ and $\pi/12$, respectively. For the Lamb–Oseen vortex model, we include parameters for three eddies with centers located at (20, 70), (50, 50), and (80, 30). Each eddy has a ring flow and core radius of 5 and a maximum radius of 80. Furthermore, we establish different obstacle scenarios in each of the two current environments.

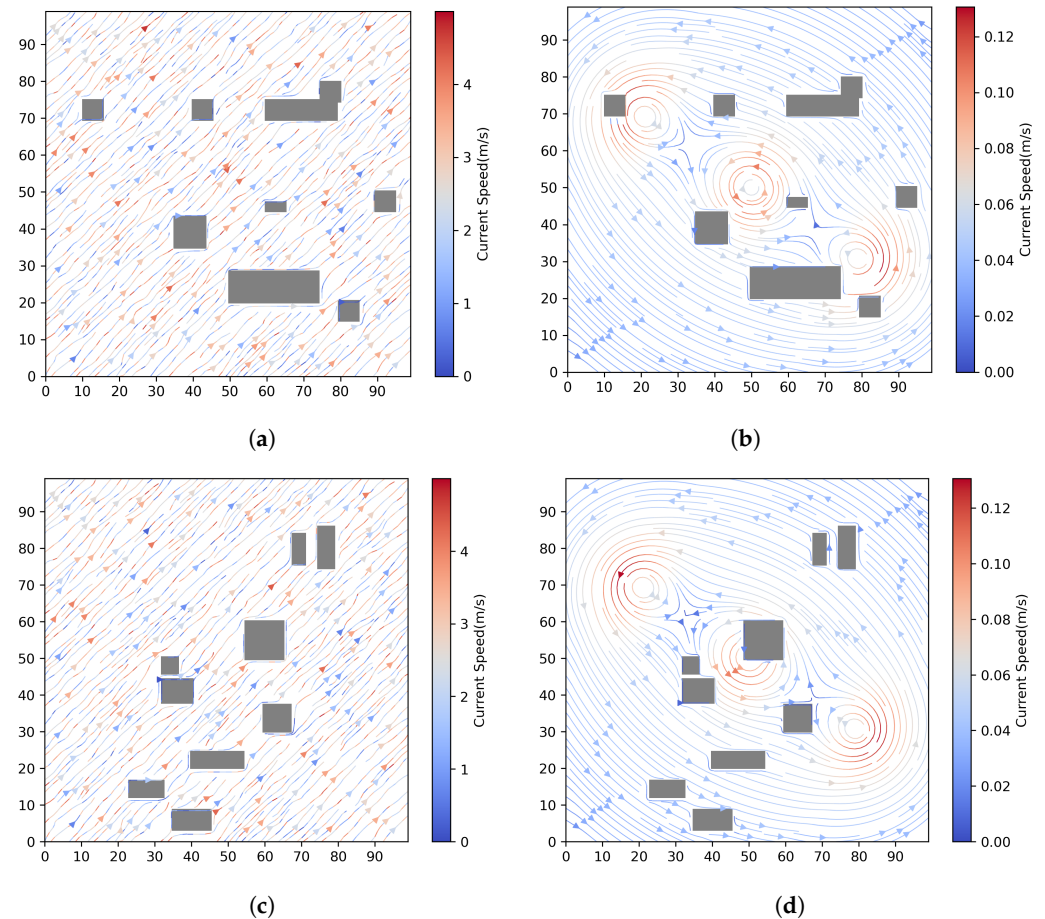


Figure 5. The four synthetic datasets; (a) Scenario A; (b) Scenario B; (c) Scenario C; (d) Scenario D.

The authentic dataset utilized in our research is sourced from the Ocean Surface Current Analyses Real-time (OSCAR) dataset (Figure 6) provided by the National Oceanic and Atmospheric Administration (NOAA) [34]. The OSCAR dataset contains ocean mixed-layer velocities, and its computation draws from satellite-derived sea surface height gradients, ocean vector wind data, sea surface temperature gradients, and simplified physical models such as Ekman and thermal wind dynamics. Covering the period from 1993 to the present day, this dataset offers daily average surface current data for the top 30 m of the ocean on a global grid with a spatial resolution of 0.25×0.25 degrees. For our experiments, we selected data randomly from a day in June 2020, which include both horizontal and vertical components of ocean current velocity. Utilizing the OSCAR dataset adds significant authenticity to our research, enhancing the validity and applicability of our algorithm by providing a real-world representation of ocean current dynamics.

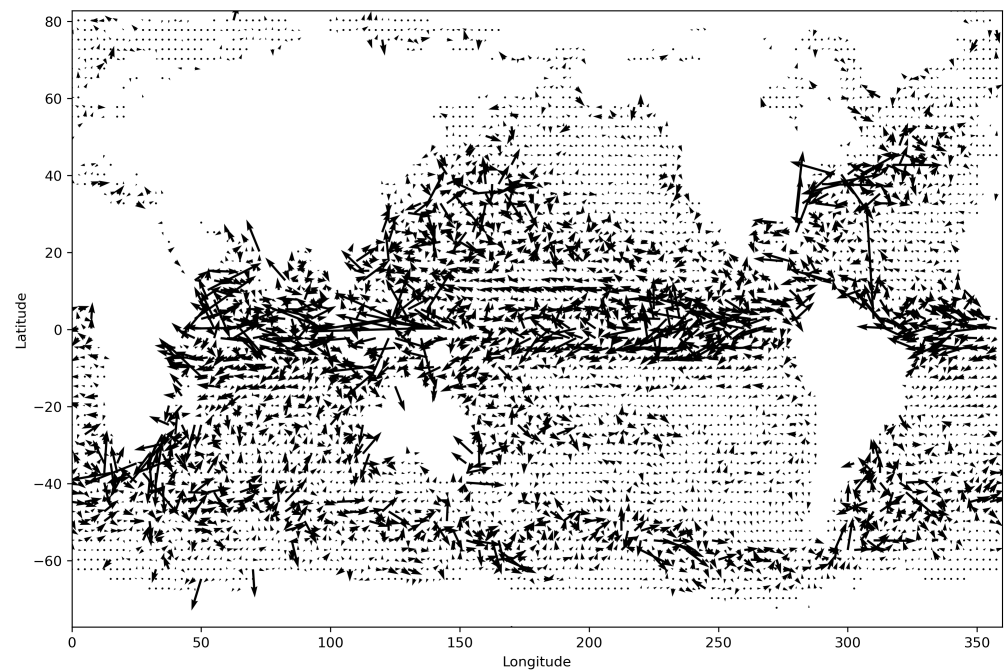


Figure 6. The OSCAR dataset is visualized with black arrows representing ocean currents. At each location where ocean currents are present, an arrow originates from that location. The direction of the arrow signifies the direction of the ocean current at that point, while the length of the arrow indicates its speed.

4.2. Path Planning

The enhanced A* is employed for path planning within the ocean current to compare with the traditional A*. Considering the trajectory of the AUV, the direction of future ocean currents is more important. Consequently, the weight of α is typically assigned a considerably higher value than that of β . Here, α is set as 10 and β as 5. The obstacle penalty weight ω_{op} is 20. In the synthetic scenarios, the departure and destination locations of the AUV are (60, 0) to (70, 80) (Figure 7a,b) and (25, 1) to (80, 95) (Figure 7c,d).

The paths planned by the enhanced A* algorithm not only focus on path distance but also significantly improve energy efficiency and safety compared to the traditional A* (Figure 7). In scenario A and scenario B, it can be seen that the enhanced A* plans different paths, which effectively solves the problem of non-conformity to ocean currents inherent in the traditional A*. In the narrow region, the problem of the traditional A* being too close to obstacles is solved, i.e., safety is improved (e.g., the path bypasses the narrow channel in the upper-right corner in Figure 7c,d).

While the enhanced A* initially adapts paths to ocean currents, these paths often lack smoothness and do not fully account for current speeds. To address this issue, we utilize the enhanced GA for further path optimization, where the path planned by the enhanced A* is selected as the initial population entity. Replication and initial mutation are performed to increase the population size and boost its diversity, preventing the population from settling into a local optimum. We can adjust the weight parameters of the fitness function based on different driving requirements and the actual ocean current conditions in the sea area. In this experiment, emphasis is placed on the smoothness and the adaptability to the ocean currents of the path. We designate regions with velocities exceeding 2.5 m/s as "high-speed areas" (0.1 m/s in scenario B and scenario D). W_1 , W_2 , W_3 , and W_4 are set as 20, 1, 20, and 1, respectively. A larger weight coefficient indicates a heightened emphasis on optimizing the corresponding aspect during the route optimization process. The parameter settings of the GA are detailed in Table 1.

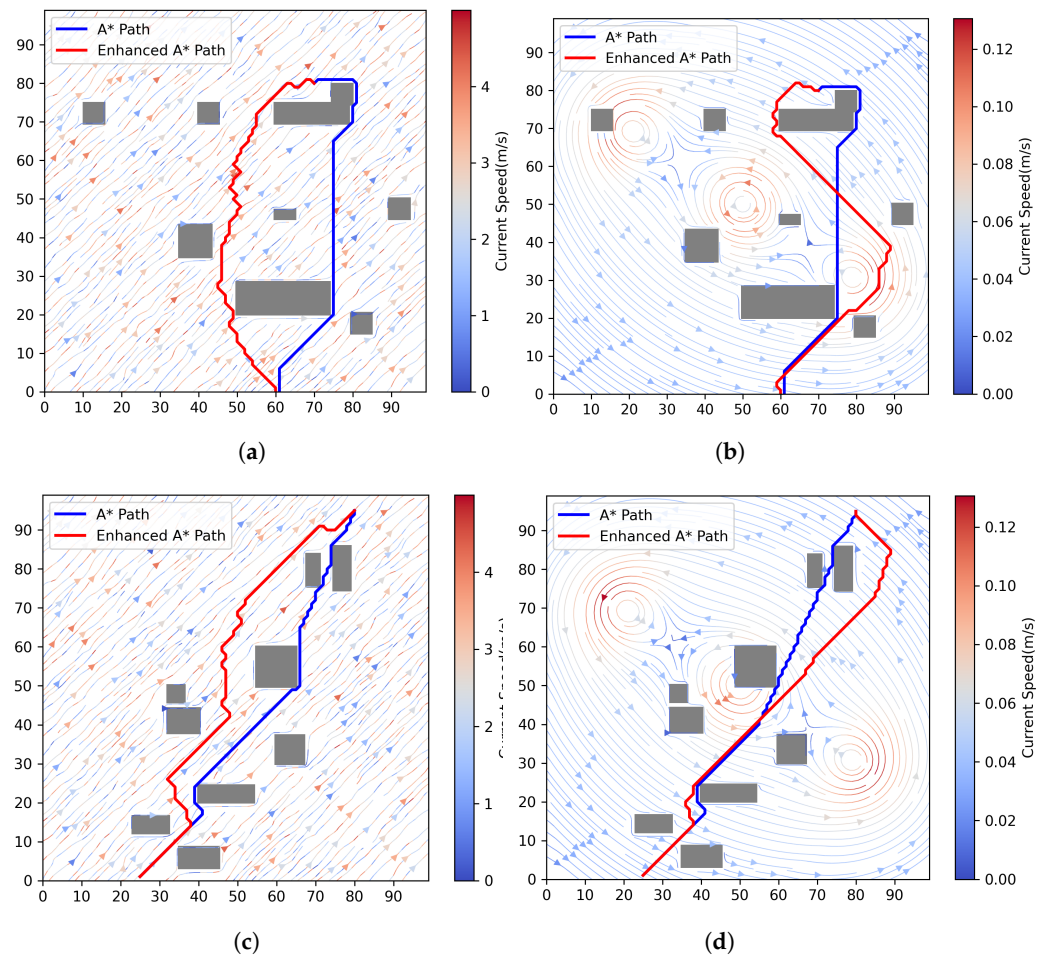


Figure 7. Simulation of enhanced A* path in the four synthetic scenarios; (a) Scenario A; (b) Scenario B; (c) Scenario C; (d) Scenario D.

Table 1. Parameters of the proposed algorithm.

Generations Number	Population Size	Mutation Rate	Tournament Individual	Tournament Size
800	200	0.1	50	20

The paths generated by the enhanced GA (Figure 8) demonstrate significant improvements in smoothness compared to those planned by the enhanced A*, specifically in the elimination of sharp turns and erratic segments. This optimization not only enhances the adaptability to ocean currents but also increases the safety of the path. We tested the proposed algorithm across four scenarios to verify its effectiveness. The results show that the final optimal path can follow the direction of the currents in a complex eddy environment, and the path avoids the narrow parts and chooses open areas that follow the direction of the currents.

The experiments were also validated on the OSCAR dataset. We set the latitude and longitude range from (116,32) to (130,41), treating land as an obstacle. The latitude and longitude coordinates of the start point are set to (120,38) and the end point to (128,33). In this experiment region, where current velocities are generally low, our focus was primarily on enhancing the smoothness and energy efficiency of the path. The final result is presented in the subsequent Figure 9.

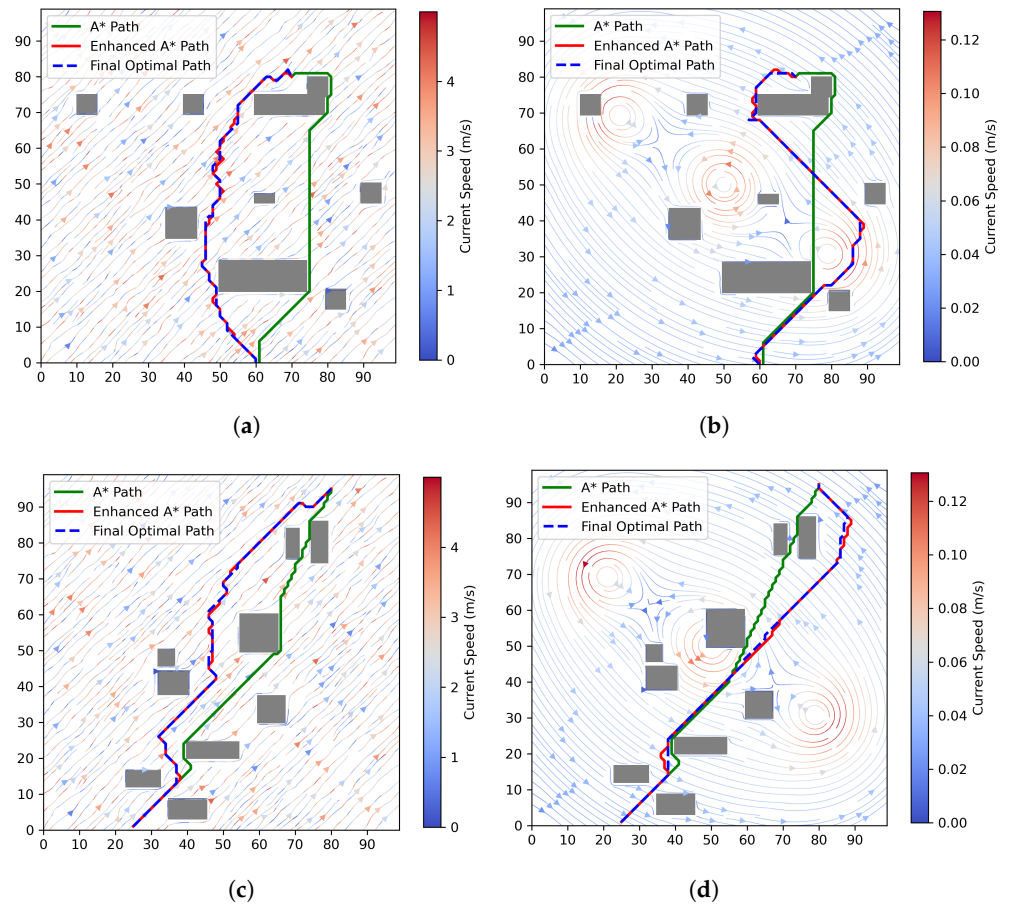


Figure 8. Simulation of final optimal path in the four synthetic scenarios; (a) Scenario A; (b) Scenario B; (c) Scenario C; (d) Scenario D.

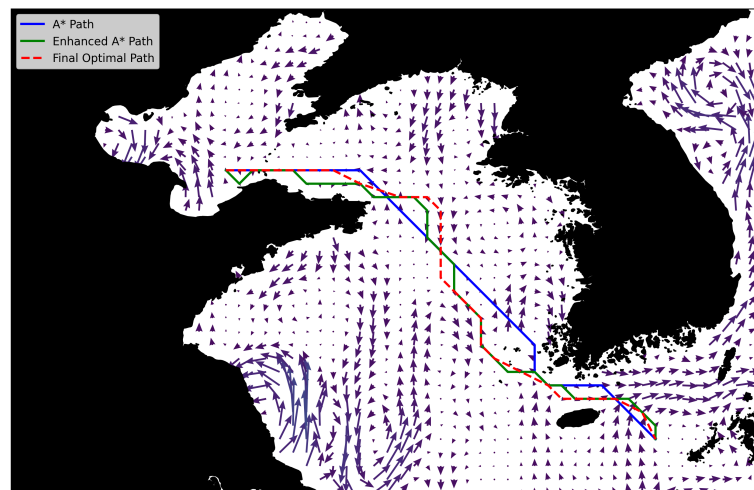


Figure 9. Comparison of path planning by using the OSCAR dataset.

The path can align with the direction of the ocean current, simultaneously enhancing path smoothness. When compared with the traditional A* path, the performance index and path rationality of the proposed algorithm significantly surpass those of A*. This aligns well with AUV path planning under the constraints of an authentic current environment, hence demonstrating that the algorithm is superior in performance in actual ocean current conditions. Our results confirmed the algorithm is able to meet the requirements of authentic ocean currents.

4.3. Three Criteria for Path Evaluation

The following three criteria characterize the advantages and disadvantages of paths obtained by various path-planning algorithms.

Smoothness: This criterion is exactly the same as the path smoothness (H) that is defined in the fitness function (Equation (14)). A lower score means a smoother path and better performance.

High-speed area (safety): This criterion calculates the score of traversing through a high-speed area (such as a fast-current zone) along a path. If the current speed at the waypoint (P_i) exceeds the threshold R , it indicates a high-speed area, and one point is added to the high-speed area score (hsa_i) (Equation (18)). When the i -th waypoint in the path is reached, the hsa_i score accumulates, eventually returning the total score for the high-speed area. A lower score means the path passes through fewer high-speed areas of ocean current, indicating better safety.

$$hsa_i = \begin{cases} 1 & \theta(V_i) > R \\ 0 & \text{otherwise} \end{cases} \quad (18)$$

Alignment with current direction (energy efficiency): This function evaluates the directional consistency of the given path with the current, which can be computed by Equation (15). For each point along the path, it calculates the included angle between the path direction and the current direction, summarizing these values using the cosine of each angle. A smaller included angle indicates greater alignment with the current, which correlates with better energy efficiency. The higher the score, the better the alignment between the path direction and ocean current direction, thus indicating superior energy efficiency for the path.

4.4. Evaluation of Path and Algorithms

Because of the scale, it is difficult to discern the details of ocean currents and paths from the visualized results of the experiments, making it difficult to visually analyze energy efficiency and safety. Therefore, we use three criteria for path evaluations. Although the path of A* looks "smoother", its turning angle is too sharp, and its adaptability to ocean currents is very low, which does not meet the path requirements of AUVs. The experimental results demonstrate that the enhanced A* algorithm not only surpasses the traditional A* in path performance but also retains its advantages. Therefore, we believe that only a comparison between the enhanced A* and the proposed algorithm is needed, which focuses on the improvement of path performance by using the GA.

We consider high-speed areas, which are the units in which the speed of the current is higher than 2.5 in scenarios A and C. In scenarios B and D, the threshold R becomes higher than 0.1. The optimized path shows the paths have significant improvements in the three aspects (smoothness, high-speed area, and alignment with current direction); therefore, we conclude that the algorithm better fulfills the requirements for an AUV path to adapt to ocean currents (Figure 10).

Applying GA optimization to the enhanced A* results in notable improvements in various performance metrics. Compared with the enhanced A*, the smoothness of the final optimal path is significantly improved, and the total path turning angle is reduced by 48%, 31%, 40%, and 35%, respectively. This substantial decrease in total path turning angles addresses a previous issue of the enhanced A* algorithm, which tended to generate paths with excessive numbers of turns and total turning angles.

Furthermore, the optimization process effectively tackles the challenge posed by high-speed areas, such as in scenarios A and C. Here, the points corresponding to high-speed ocean currents decrease by 16% and 6%, respectively. By accounting for these high-speed areas, the optimized path significantly improves path safety. In scenarios B and D, where high-speed areas are minimal, the need for optimizing path safety is limited, resulting in

unchanged safety performance before and after optimization. In all scenarios, the optimized path shows improved alignment with current direction, with increases of 7%, 50%, 3%, and 2%, respectively. Particularly noteworthy is the alignment achieved in scenario B, where the path closely follows the Lamb–Oseen vortex, creating a beneficial downstream effect. This demonstrates how GA optimization builds upon the adaptive capabilities of the enhanced A* algorithm, further enhancing its ability to navigate ocean currents effectively.

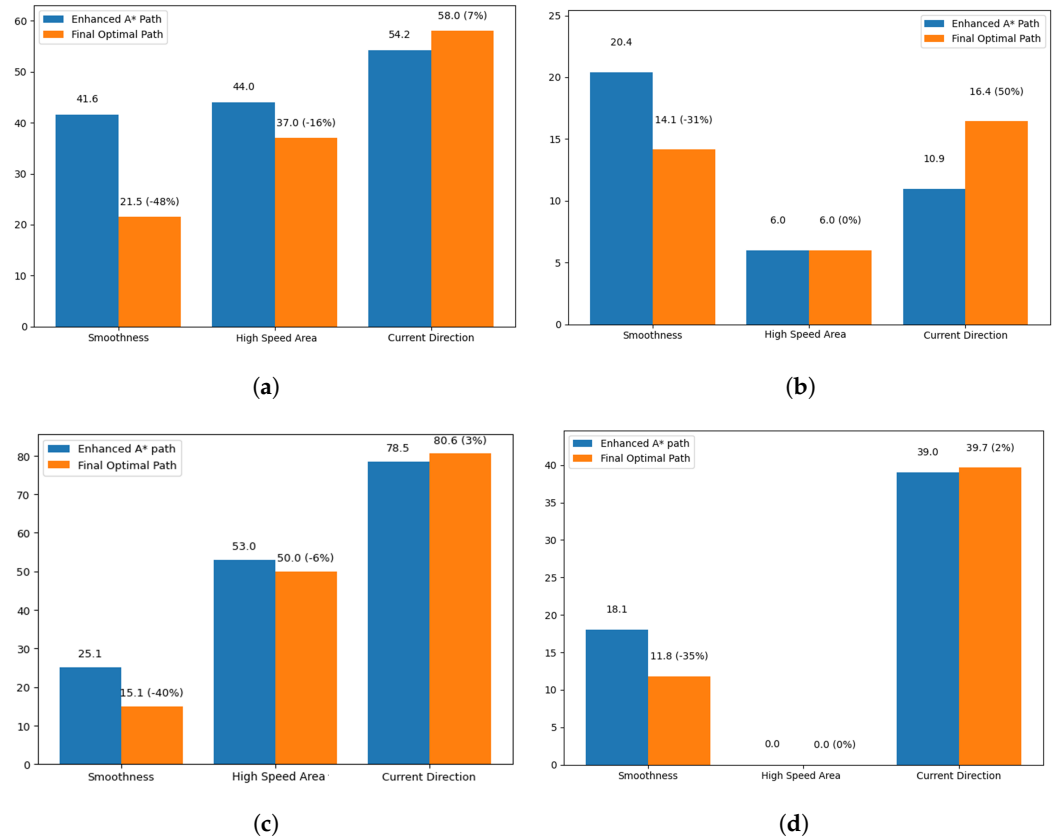


Figure 10. Path performances in the four synthetic scenarios; (a) Scenario A; (b) Scenario B; (c) Scenario C; (d) Scenario D.

In experiments using the OSCAR dataset, areas with velocities exceeding 0.03 m/s were defined as “high-speed areas”. Comparisons between the enhanced A* algorithm and the proposed algorithm reveal notable improvements: smoothness increased by 67%, the high-speed area decreased by 8%, and alignment with current direction improved by 8% (Figure 11). These results highlight the effectiveness of GA optimization in reducing total turning angles, improving safety by reducing high-speed areas, and enhancing energy efficiency through better alignment with ocean currents. Therefore, we conclude that the proposed algorithm exhibits superior path performance across authentic ocean current datasets, demonstrating its efficacy in real-world scenarios.

To ensure stability, we set the random seed to 49 and conducted 20 repeated experiments. The results, detailed in Table 2, indicate that the proposed algorithm can stably improve the performance, enabling the AUV to find paths that are better aligned with the ocean current environment.

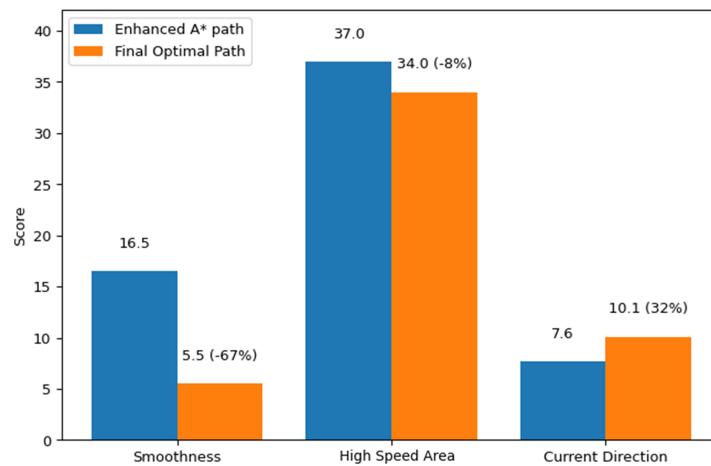


Figure 11. Path performance comparison in the authentic ocean current dataset.

Table 2. Performance of different algorithms.

	The Proposed Algorithm			Enhanced A*
	Average	Variance	Maximum	
Smoothness	24	4.5	19.6	41.6
High-speed area	41.4	6	37	44
Current direction	58.7	1.6	61.3	54.2

5. Conclusions and Future Work

This research presents a path-planning algorithm tailored for AUVs, which takes into account the intricate influence and constraints posed by ocean currents. This algorithm amalgamates the strengths of both A* and the GA. The key components encompass enhancing the cost function of A* and utilizing its output as an initial population, crafting a fitness function tailored to the prevailing ocean current conditions, employing adaptive mutation within the GA framework to further optimize path performance, and culminating in a path. We establish quantitative evaluation metrics for path planning and conduct performance comparisons in both simulated and authentic ocean current environments. Our experimental results demonstrate a substantial improvement over traditional path-planning methodologies in terms of path smoothness, energy efficiency, and safety. This underscores the practical value and applicability of our approach in real-world AUV applications.

It is essential to acknowledge that our study simplifies the AUV and ocean currents into two-dimensional models, overlooking the complexities of dynamic models and three-dimensional path planning. In three-dimensional space, path planning entails not only horizontal movement but also vertical ascent and descent, necessitating the consideration of a broader spectrum of dynamic and static obstacles. Our future work will delve into advanced obstacle-avoidance algorithms to enable AUVs to navigate flexibly within intricate 3D environments, such as evading collisions with floating objects or challenging terrain. The overarching goal is to ensure that AUVs can reach their destinations swiftly and safely while minimizing fuel consumption.

Additionally, path planning for the swarm is emerging as a pivotal development direction in AUV applications, in which the coordination strategy among AUVs plays a critical role. This includes aspects such as resource sharing, task allocation, and collision avoidance. In our future research, we intend to explore advanced collaborative path-planning algorithms to guarantee the efficient and secure operation of AUV swarms. Moreover, we plan to apply the algorithm presented in this paper to practical AUV missions such as underwater exploration, aiming to advance the field of AUV path planning and foster innovation in underwater robotics.

Author Contributions: Conceptualization, Z.C. and J.Y.; methodology, Z.C., Y.G. and J.Y.; software, Z.C. and R.H.; writing—original draft preparation, Z.C. and R.H.; writing—review and editing, J.Y. and W.Y.; visualization, Z.C. and Y.G.; supervision, J.Y. and X.P.; project administration, X.P.; funding acquisition, J.Y. All authors have read and agreed to the published version of the manuscript.

Funding: The financial support for this work comes from the Shandong Province Natural Science Foundation Youth Branch (ZR2022QD121).

Data Availability Statement: Data are contained within the article.

Conflicts of Interest: The authors declare no conflicts of interest.

References

1. Paull, L.; Saeedi, S.; Seto, M.; Li, H. AUV Navigation and Localization: A Review. *IEEE J. Ocean. Eng.* **2014**, *39*, 131–149. [\[CrossRef\]](#)
2. Mujeebu, M.A. The disappearance of MH370 and the search operations—The role of technology and emerging research challenges. *IEEE Aerosp. Electron. Syst. Mag.* **2016**, *31*, 6–16. [\[CrossRef\]](#)
3. Cheng, C.; Sha, Q.; He, B.; Li, G. Path planning and obstacle avoidance for AUV: A review. *Ocean Eng.* **2021**, *235*, 109355. [\[CrossRef\]](#)
4. Liang, S.; Zhi-Ming, Q.; Heng, L. A Survey on Route Planning Methods of AUV Considering Influence of Ocean Current. In Proceedings of the 2018 IEEE 4th International Conference on Control Science and Systems Engineering (ICCSSE), Wuhan, China, 21–23 August 2018; pp. 288–295. [\[CrossRef\]](#)
5. Saad, M.; Salameh, A.I.; Abdallah, S. Energy-Efficient Shortest Path Planning on Uneven Terrains: A Composite Routing Metric Approach. In Proceedings of the 2019 IEEE International Symposium on Signal Processing and Information Technology (ISSPIT), Ajman, United Arab Emirates, 10–12 December 2019; pp. 1–6. [\[CrossRef\]](#)
6. Heo, Y.J.; Chung, W.K. RRT-based path planning with kinematic constraints of AUV in underwater structured environment. In Proceedings of the 2013 10th International Conference on Ubiquitous Robots and Ambient Intelligence (URAI), Jeju, Republic of Korea, 30 October–2 November 2013; pp. 523–525. [\[CrossRef\]](#)
7. Fu-guang, D.; Peng, J.; Xin-qian, B.; Hong-jian, W. AUV local path planning based on virtual potential field. In Proceedings of the IEEE International Conference Mechatronics and Automation, Niagara Falls, ON, Canada, 29 July–1 August 2005; Volume 4, pp. 1711–1716. [\[CrossRef\]](#)
8. Fan, X.; Xue, C.; Zhou, H. Research on UUV path planning method based on bidirectional A* algorithm. In Proceedings of the 2022 China Automation Congress (CAC), Xiamen, China, 25–27 November 2022; pp. 1141–1144. [\[CrossRef\]](#)
9. Carroll, K.; McClaran, S.; Nelson, E.; Barnett, D.; Friesen, D.; William, G. AUV path planning: An A* approach to path planning with consideration of variable vehicle speeds and multiple, overlapping, time-dependent exclusion zones. In Proceedings of the 1992 Symposium on Autonomous Underwater Vehicle Technology, Washington, DC, USA, 2–3 June 1992; pp. 79–84. [\[CrossRef\]](#)
10. Wang, L.; Pang, S. Chemical Plume Tracing using an AUV based on POMDP Source Mapping and A-star Path Planning. In Proceedings of the OCEANS 2019 MTS/IEEE SEATTLE, Seattle, WA, USA, 27–31 October 2019; pp. 1–7. [\[CrossRef\]](#)
11. Li, F.; Wu, L.; Shi, L.; Cao, X.; Zhang, X.; Zeng, G. UUV Dynamic Path Planning Algorithm Based on A-Star and Dynamic Window. In *Proceedings of the International Conference on Bio-Inspired Computing: Theories and Applications*; Springer: Singapore, 2023; pp. 159–170.
12. Lefebvre, N.; Schjøberg, I.; Utne, I.B. Integration of risk in hierarchical path planning of underwater vehicles. *IFAC-PapersOnLine* **2016**, *49*, 226–231. [\[CrossRef\]](#)
13. Zhang, G.L.; Jia, H.M. Global path planning of AUV based on improved ant colony optimization algorithm. In Proceedings of the 2012 IEEE International Conference on Automation and Logistics, Zhengzhou, China, 15–17 August 2012; pp. 606–610. [\[CrossRef\]](#)
14. Tang, X.; Yu, F.; Chen, R. Path planning of underwater vehicle based on particle swarm optimization. In Proceedings of the 2010 International Conference on Intelligent Control and Information Processing, Dalian, China, 13–15 August 2010; pp. 123–126. [\[CrossRef\]](#)
15. Zeng, Z.; Sammut, K.; Lian, L.; He, F.; Lammas, A.; Tang, Y. A comparison of optimization techniques for AUV path planning in environments with ocean currents. *Robot. Auton. Syst.* **2016**, *82*, 61–72. [\[CrossRef\]](#)
16. Cheng, C.T.; Fallahi, K.; Leung, H.; Tse, C.K. A Genetic Algorithm-Inspired UUV Path Planner Based on Dynamic Programming. *IEEE Trans. Syst. Man Cybern. Part C* **2012**, *42*, 1128–1134. [\[CrossRef\]](#)
17. Cao, J.; Li, Y.; Zhao, S.; Bi, X. Genetic-Algorithm-Based Global Path Planning for AUV. In Proceedings of the 2016 9th International Symposium on Computational Intelligence and Design (ISCID), Hangzhou, China, 10–11 December 2016; Volume 2, pp. 79–82. [\[CrossRef\]](#)
18. Yan, S.; Pan, F. Research on Route Planning of AUV Based on Genetic Algorithms. In Proceedings of the 2019 IEEE International Conference on Unmanned Systems and Artificial Intelligence (ICUSAI), Xi'an, China, 22–24 November 2019; pp. 184–187. [\[CrossRef\]](#)

19. Ma, Y.; Mao, Z.; Wang, T.; Qin, J.; Ding, W.; Meng, X. Obstacle avoidance path planning of unmanned submarine vehicle in ocean current environment based on improved firework-ant colony algorithm. *Comput. Electr. Eng.* **2020**, *87*, 106773. [[CrossRef](#)]
20. Yao, P.; Zhao, S. Three-Dimensional Path Planning for AUV Based on Interfered Fluid Dynamical System Under Ocean Current (June 2018). *IEEE Access* **2018**, *6*, 42904–42916. [[CrossRef](#)]
21. Chu, Z.; Wang, F.; Lei, T.; Luo, C. Path Planning Based on Deep Reinforcement Learning for Autonomous Underwater Vehicles Under Ocean Current Disturbance. *IEEE Trans. Intell. Veh.* **2023**, *8*, 108–120. [[CrossRef](#)]
22. Zhu, D.; Yang, S.X. Bio-Inspired Neural Network-Based Optimal Path Planning for UUVs Under the Effect of Ocean Currents. *IEEE Trans. Intell. Veh.* **2022**, *7*, 231–239. [[CrossRef](#)]
23. Sun, Y.; Gu, R.; Chen, X.; Sun, R.; Xin, L.; Bai, L. Efficient time-optimal path planning of AUV under the ocean currents based on graph and clustering strategy. *Ocean. Eng.* **2022**, *259*, 111907. [[CrossRef](#)]
24. Hao, K.; Zhao, J.; Li, Z.; Liu, Y.; Zhao, L. Dynamic path planning of a three-dimensional underwater AUV based on an adaptive genetic algorithm. *Ocean. Eng.* **2022**, *263*, 112421. [[CrossRef](#)]
25. Wen, J.; Yang, J.; Wang, T. Path Planning for Autonomous Underwater Vehicles Under the Influence of Ocean Currents Based on a Fusion Heuristic Algorithm. *IEEE Trans. Veh. Technol.* **2021**, *70*, 8529–8544. [[CrossRef](#)]
26. Elfes, A. Using occupancy grids for mobile robot perception and navigation. *Computer* **1989**, *22*, 46–57. [[CrossRef](#)]
27. Tang, H.; Nichols, C.R.; Wright, L.D.; Resio, D. Modeling Multiscale and Multiphysics Coastal Ocean Processes: A Discussion on Necessity, Status, and Advances. *J. Mar. Sci. Eng.* **2021**, *9*, 847. [[CrossRef](#)]
28. Saffman, P.G. *Vortex Dynamics*; Cambridge University Press: Cambridge, UK, 1995.
29. Li, J.; Li, C.; Chen, T.; Zhang, Y. Improved RRT algorithm for AUV target search in unknown 3D environment. *J. Mar. Sci. Eng.* **2022**, *10*, 826. [[CrossRef](#)]
30. Lee, J.; Kim, D.W. An effective initialization method for genetic algorithm-based robot path planning using a directed acyclic graph. *Inf. Sci.* **2016**, *332*, 1–18. [[CrossRef](#)]
31. Srinivas, M.; Patnaik, L. Adaptive probabilities of crossover and mutation in genetic algorithms. *IEEE Trans. Syst. Man Cybern.* **1994**, *24*, 656–667. [[CrossRef](#)]
32. Patil, S.; Bhende, M. Comparison and analysis of different mutation strategies to improve the performance of genetic algorithm. *IJCSIT Int. J. Comput. Sci. Inf. Technol.* **2014**, *5*, 4669–4673.
33. Tang, P.H.; Tseng, M.H. Adaptive directed mutation for real-coded genetic algorithms. *Appl. Soft Comput.* **2013**, *13*, 600–614. [[CrossRef](#)]
34. Dohan, K. Ocean Surface Current Analyses Real-time (OSCAR) Surface Currents—Interim 0.25 Degree, Version 2.0. 2021. Available online : https://podaac.jpl.nasa.gov/dataset/OSCAR_L4_OC_INTERIM_V2.0 (accessed on 22 May 2023).

Disclaimer/Publisher’s Note: The statements, opinions and data contained in all publications are solely those of the individual author(s) and contributor(s) and not of MDPI and/or the editor(s). MDPI and/or the editor(s) disclaim responsibility for any injury to people or property resulting from any ideas, methods, instructions or products referred to in the content.